Available online at www.sciencedirect.com
SCIENCE DIRECT®
International Journal of Heat and Mass Transfer 48 (2005) 5017–5035
International Journal of HEAT and MASS TRANSFER
www.elsevier.com/locate/ijhmt

Film cooling characteristics of rows of round holes at various streamwise angles in a crossflow: Part II. Heat transfer coefficients

C.H.N. Yuen, R.F. Martinez-Botas *

Department of Mechanical Engineering, Imperial College of Science, Technology and Medicine, London, United Kingdom

Received 1 January 2003; received in revised form 12 July 2003
Available online 10 August 2005

Abstract

Measurements of heat transfer coefficient (h) are presented for rows of round holes at streamwise angles of 30°, 60° and 90° with a short but engine representative hole length ($L/D = 4$). The study began with a single row of holes with pitch-to-diameter ratios of 3 and 6, followed by two inline and staggered rows for each hole spacing and streamwise inclination, which amount to 105 different test cases in addition to the 21 test cases presented on the single hole [C.H.N. Yuen, R.F. Martinez-Botas, Film cooling characteristics of a single round hole at various angles in a crossflow: Part I. Effectiveness, Int. J. Heat Mass Transfer, in press; C.H.N. Yuen, R.F. Martinez-Botas, Film cooling characteristics of a single round hole at various angles in a crossflow: Part II. Heat transfer coefficients, Int. J. Heat Mass Transfer, in press]. The present investigation is a continuation of the previous work [Yuen and Martinez-Botas, Parts I and II, in press] with the same test facility, operating conditions (freestream Reynolds number, Re_D of 8563, and blowing ratio, $0.33 \leqslant M \leqslant 2$), and measurement technique of liquid crystal thermography and the steady-state heat transfer method, therefore the results presented in the form of h/h_0, which is the ratio of heat transfer coefficient with film cooling to that without, are directly comparable. Both local values and laterally averaged ones are presented, the latter refers to the averaged value across the central hole. The corresponding measurements of effectiveness for the rows of holes are presented in a companion paper [C.H.N. Yuen, R.F. Martinez-Botas, Film cooling characteristics of rows of round holes at various angles in a crossflow: Part I. Effectiveness, Int. J. Heat Mass Transfer, submitted for publication]. The low effectiveness observed with the 90° holes in the companion paper [Yuen and Martinez-Botas, submitted for publication] and the relatively large heat transfer coefficient presented here, suggest that the normal injection should only be used in situations where shallower holes are not feasible. The combined performance of effectiveness and heat transfer coefficient suggests that the two inline rows are likely to be advantageous in the film cooling of turbine blades with good coverage per unit mass flow of cooling air and lower thermal stresses due to the smaller heat load.

* Corresponding author. Tel.: +44 20 75947241; fax: +44 20 78238845.
E-mail address: r.botas@ic.ac.uk (R.F. Martinez-Botas).

0017-9310/$ - see front matter © 2005 Elsevier Ltd. All rights reserved.
doi:10.1016/j.ijheatmasstransfer.2005.05.020

Nomenclature

D	hole diameter, 10 mm
h	heat transfer coefficient in the presence of film cooling ($W/m^2 K$), $h = q''/(T_w - T_{aw})$ where T_{aw} is substituted by T_∞ when $T_2 = T_\infty$
h_0	heat transfer coefficient in the absence of film cooling ($W/m^2 K$), $h_0 = q''/(T_{w0} - T_\infty)$
L	hole length
M	blowing ratio ($\rho_2 U_2/\rho_\infty U_\infty$)
p	hole pitch
q''	wall heat flux (W/m^2)
Re_D	Reynolds number ($\rho_\infty U_\infty D/\mu_\infty$)
s	row spacing
T	temperature (K)
TLC	thermographic liquid crystals
U	velocity (m/s)
x	coordinate: streamwise (axial) direction (see Figs. 1 and 2)
y	coordinate: vertical (height-wise) direction (see Fig. 2)
z	coordinate: lateral direction (see Fig. 1)

Greek symbols

δ	boundary layer thickness
δ^*	displacement thickness, $\delta^* = \int_0^\delta \left(1 - \frac{U}{U_\infty}\right) dy$
δ_i	momentum thickness, $\delta_i = \int_0^\delta \left(1 - \frac{U}{U_\infty}\right) \frac{U}{U_\infty} dy$
ρ	density (kg/m^3)

Subscripts

∞	freestream
0	in the absence of film cooling
2	coolant or secondary injection
aw	adiabatic wall
w	wall
Overbar	laterally-averaged

1. Introduction

Film cooling is required to achieve the required life span of turbine blades under adverse centrifugal and thermal stress levels resulted from the demand of high temperature-rise combustors with turbine entry temperatures doubled in the past 25 years. It is essential to improve cooling designs to keep the temperature level and thermal gradients in various turbine components within acceptable limits using minimum cooling air.

Aerodynamic and thermal procedures currently available to turbine designers do not permit a priori designs that achieve design goals without expensive development iterations. The current study expands the database of reliable measurements which is much anticipated in the construction of reliable correlations for the application of film cooling in gas turbine industries, by systematically adding 105 test cases to the 21 cases presented on single round holes [1,2]. Another advantage of this extended study is that all results are directly comparable as they were measured in the same facility, with the same operating conditions and technique.

Studies of heat transfer with film cooling on a row of holes with a streamwise inclination of 30° or 35° and a pitch-to-diameter ratio of 3 on a flat plate shown in Fig. 1 were described [4–10]. The latter study showed it is important to have information of the film cooling effectiveness and the heat transfer coefficient. In general, heat transfer coefficient downstream of a row of holes increased with increasing blowing ratio, because the pressure deficit created by the detached jets caused the freestream to enter the region below the jet, and increased the heat transfer rate locally.

The behaviour of multiple jets differs from that of a single jet, and the interaction between adjacent jets varies with blowing ratio and the pitch-to-diameter ratio. Pietrzyk et al. [11] studied a row of 35° jets with a hole length-to-diameter ratio of 3.5 and a pitch-to-diameter ratio of 3, similar to one of the current arrangements, and found that the strength of the longitudinal vortices scaled with velocity ratio and increasing distance. Furthermore, the turbulence intensity was increased through the disturbance added by the multiple jets. Sinha et al. [12] studied two rows of 35° holes with a pitch-to-diameter ratio of 3 and a row spacing-to-diameter ratio of 40, and showed that the upstream row reduced the momentum of the crossflow and the velocity gradients in the shear layers, and lowered the turbulence level for the second row.

The effects of the hole length have been studied by Burd and Simon [13,14], Brundage et al. [15] and Walters and Leylek [16], and some of the findings have been reported in [1–3,17], and are summarised here. In general, short holes are subject to skewed jet velocity profiles with a maximum value greater than that of a turbulent jet for the same mass flow in the downstream half of the hole, with low blowing ratios. This non-uniform velocity distribution of the exiting depends on the hole geometry and the blowing ratio. Lloyd and Brown [18] and Andrews et al. [19] concluded that short holes may give rise to greater heat transfer than longer holes.

The definition of heat transfer coefficient, h, is given in the *Nomenclature* section. The objective of film cooling is to achieve low heat transfer from the surrounding hot mainstream to the turbine blades, and large effectiveness on the blade surface. The interpretation of wall

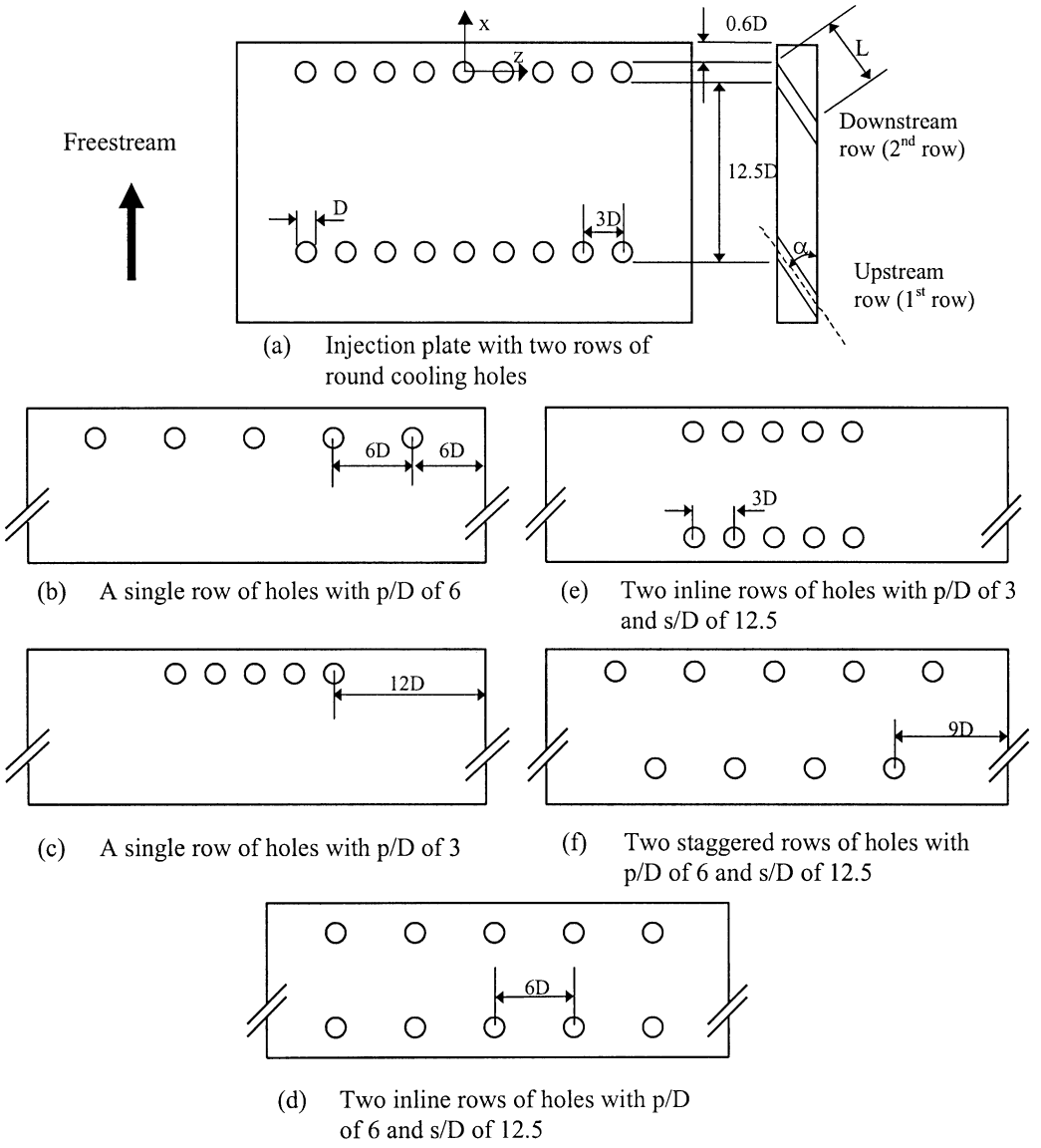

Fig. 1. Geometries and arrangements of cooling holes at streamwise angle, α.

measurements of temperature such as these reported in this paper benefits from knowledge of local velocities and wall pressures reviewed in Yuen and Martinez-Botas [1,3], and will not be repeated here.

2. Experimental apparatus and procedure

The test facility and measurement technique are consistent with the previous studies of Yuen and Martinez-Botas [2] and Yuen [17], and will only be described briefly here for the sake of completeness. The technique implemented is liquid crystal thermography and the steady-state heat transfer method with encapsulated liquid crystal of a bandwidth of 10 °C.

Fig. 2 shows a schematic of the test rig. The test section comprised of a knife bleed, an injection plate and a test plate with a constant heat flux, the details of which are described in the following paragraphs.

The knife bleed controls the origin of the freestream boundary layer in the test section, and the sandpaper on the knife bleed trips it. Three injection plates with cooling holes at 30°, 60° and 90° were made of Perspex, and each plate contained two rows (12.5 diameters apart) of nine cylindrical holes of the same inclination, Fig. 1. The upstream row was covered for the tests with a single

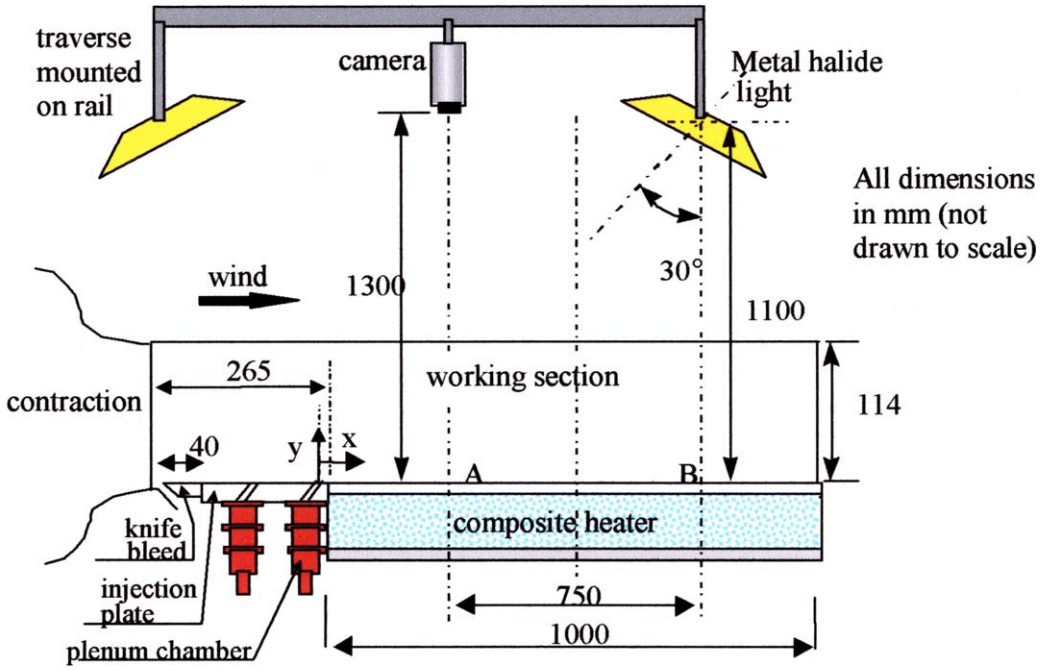

Fig. 2. Experimental set-up.

row, and the appropriate holes were taped to simulate the required pitch-to-diameter ratios of 3 and 6. For all test cases, each row of jets stemmed from five cooling holes, except for the upstream row of the two staggered rows, which had four, Fig. 1. The downstream row of holes was positioned as close as possible to the downstream edge of the injection plate, such that the trailing edge of the holes was 6 mm from the downstream edge of test plate, which was desirable from the view point of measurements.

Fig. 3 illustrates the composite heater plate immediately downstream of the injection plate, and Table 1

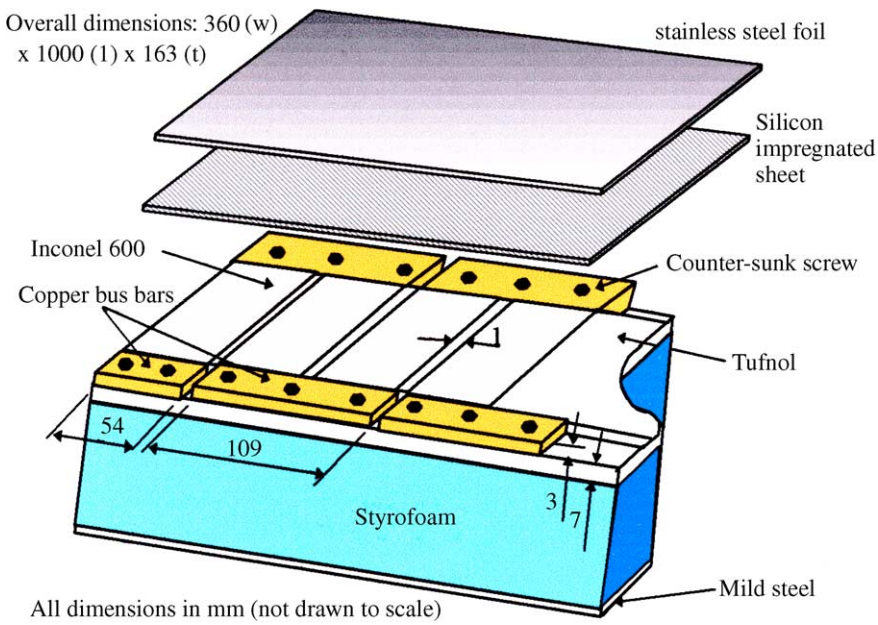

Fig. 3. Test plate with a constant heat flux.

Table 1
Materials in the test plate

Order	Materials	Thermal conductivity (W/m K)	Functions
Top	0.2 mm Stainless steel 304 Foil	14.9	• Convective heat transfer surface
	0.2 mm Thick silicon impregnated sheet	0.79	• Thermal conductance • Electrical insulation
	0.08 mm Thick Inconel 600	14.8	• Heating element
	10 mm Tufnol (kite brand)	0.26	• Thermal insulation • Mechanical support
	15 cm Styrofoam	0.027	• Thermal insulation
Bottom	3 mm Mild steel	60	• Mechanical support

Table 2
Test cases (105 in total)

Streamwise angles (°)	Configurations	No. of blowing holes in each row	p/D	s/D	Blowing ratio (M)
30, 60 and 90	One row Two inline rows	5	3 and 6	12.5	0.33, 0.5, 0.67, 1.0, 1.33, 1.67 and 2.0
	Two staggered rows	4 in the upstream row 5 in the downstream row	6		

Table 3
Boundary layer characteristics

Position (δ/D)	Boundary layer thickness	Displacement thickness (δ^*/D)	Momentum thickness (δ_i/D)
Injection plane ($x/D = 0$)	1	0.15	0.11

summarises the layers of the composite plate. The reasons that this heating arrangement was selected were described in detail in Yuen and Martinez-Botas [2] and Yuen [17]. Briefly, this arrangement minimises the effects of any non-uniform resistance to achieve an even heat flux distribution. Ten T-type (copper–constantan) thermocouples of standard gage 39–40 were installed under the uppermost convective test surface. The composite heater plate was powered by a single phase transformer and controlled by a variac. The uniformity of heat flux was further verified at different electrical settings, and the results were satisfactory.

The laboratory compressed air was filtered, regulated by a needle valve and monitored by a rotameter before entering the plenum chamber and the cooling holes. The jet temperature was measured by a T-type (copper–constantan) thermocouple at the cooling hole entrance and exit, and the temperature was 20 °C ± 0.1 °C approximately.

The imaging system used is identical to that used in Yuen and Martinez-Botas [1]. It comprised of a colour

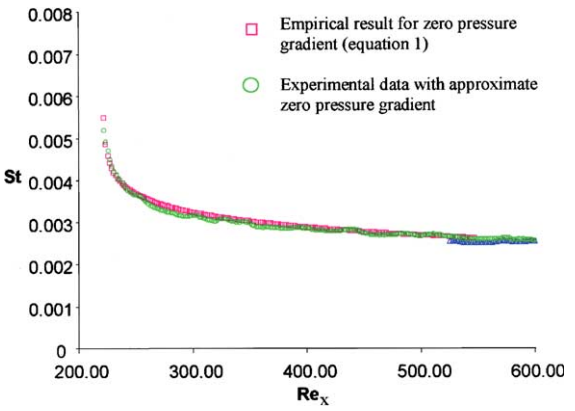

Fig. 4. Distribution of Stanton number with Reynolds number in the absence of film cooling.

JVC CCD camera, two light sources, and a 24-bit frame grabber installed in a computer. The temperature and hue calibration for the liquid crystals, the image capture procedures and the data reduction method used are also the same as those employed in the previous studies [1–3].

2.1. Experimental uncertainty

Corrections are applied to consider heat loss through thermocouple leads using the method proposed by Schneider [20]. Radiation from the heated test surface coated with liquid crystals and conduction out the back of the test surface have been evaluated and subtracted from the average heat generated within the heater to give the corrected net local heat flux. The uncertainty in h/h_0 is evaluated by the method of Kline and McClintock [21], and is approximately ±7%.

2.2. Operating conditions

The freestream velocity, temperature and turbulence intensity were 13 m/s, 20 °C and 2.7% respectively. The freestream Reynolds number based on the hole diameter and freestream velocity, Re_D, was 8563. The injectant-to-freestream blowing ratio varied from 0.33 to 2. The heat transfer tests were conducted with a constant heat flux of 410 W/m^2 and with the injectant at 20 °C ($\rho_2/\rho_\infty = 1$). The test cases investigated in the current study are listed in Table 2. Table 3 provides the boundary layer characteristics.

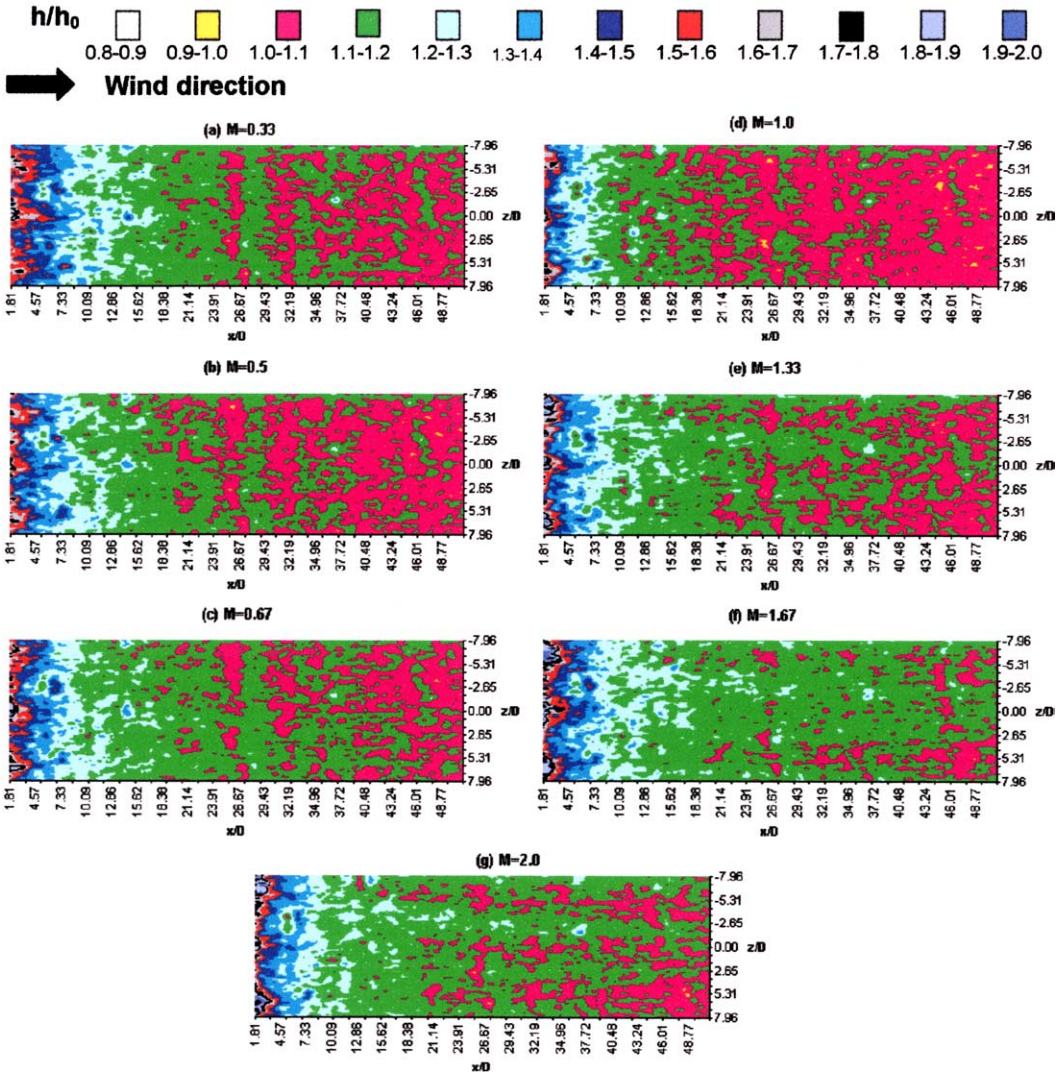

Fig. 5. Distribution of heat transfer coefficient, h/h_0, for a row of 30° holes with p/D of 6 (only the centre 3 are shown).

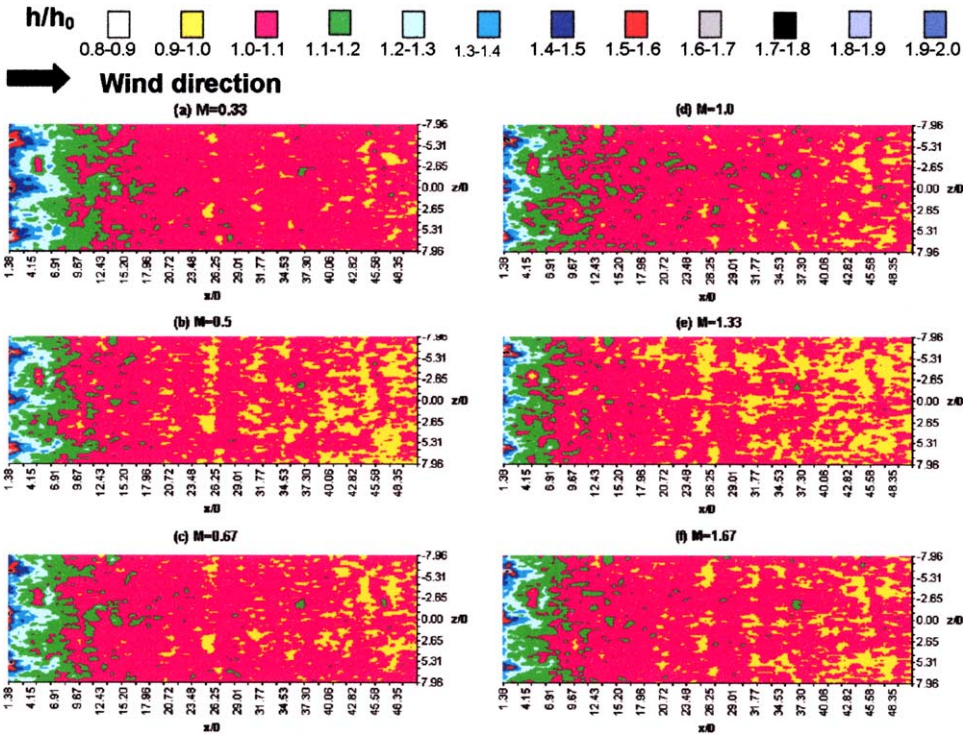

Fig. 6. Distribution of heat transfer coefficient, h/h_0, for a row of 60° holes with p/D of 6 (only the centre 3 are shown).

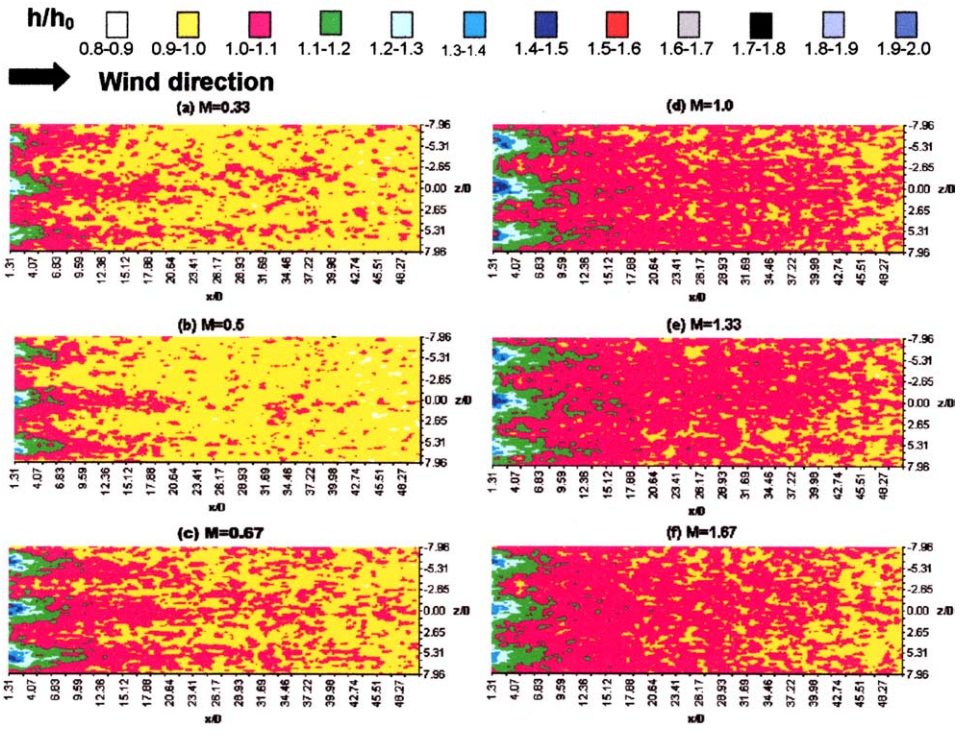

Fig. 7. Distribution of heat transfer coefficient, h/h_0, for a row of 90° holes with p/D of 6 (only the centre 3 are shown).

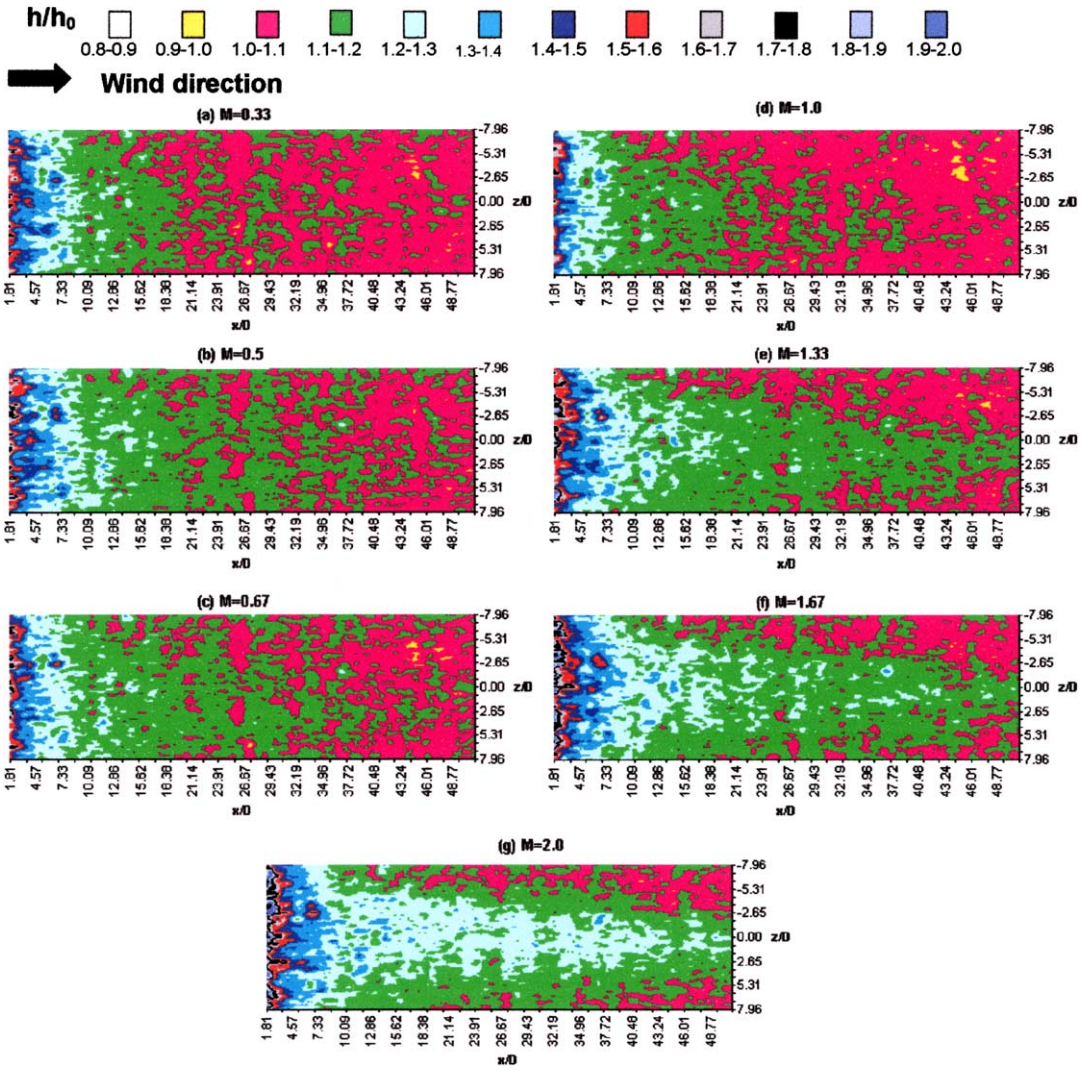

Fig. 8. Distribution of heat transfer coefficient, h/h_0, for a row of 30° holes with p/D of 3.

2.3. Non-filmed–cooled heat transfer

A well accepted approximation of heat transfer in a turbulent boundary layer for a constant freestream velocity flow along a semi-infinite plate with an arbitrarily specified heat flux and unheated starting length is given in Eq. (1). The non-filmed–cooled heat transfer tests were conducted with the holes covered with thin tape, and the results can be expressed in terms of Stanton number, according to Eq. (2). There was an excellent agreement between the empirical and experimental results with the approximate zero pressure gradient, Fig. 4.

$$St = 0.03Pr^{-0.4}Re_x^{-0.2}\left[1-\left(\frac{\xi}{x}\right)^{0.9}\right]^{-1/9} \tag{1}$$

where St is the local Stanton number, Pr is Prandtl number, $\mu C_p/k$, C_p is the specific heat of freestream at constant pressure (J/kg K), Re_x is the freestream Reynolds number, $\rho U_\infty x/\mu$, x is the axial distance starting from the origin of boundary layer (m), μ is the freestream dynamic viscosity coefficient (N s/m^2), and ξ is the unheated starting length (m). The Stanton number is defined as,

$$St = \frac{q''}{\rho C_p U_\infty (T_{w0} - T_\infty)} \tag{2}$$

where q'' is the local heat flux per unit area on heated plate (W/m^2), ρ is the freestream density (kg/m^3), C_p is the specific heat of the freestream at constant pressure (J/kg K), U_∞ is the free-stream velocity (m/s), T_{w0} is the local wall temperature in the absence of film cooling

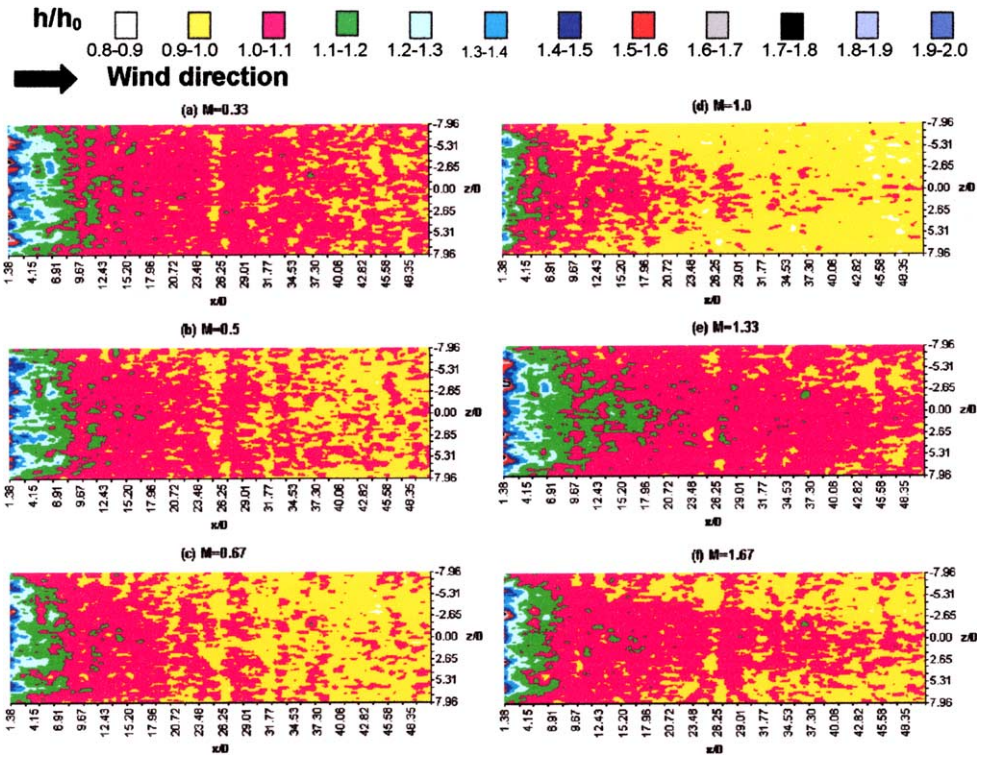

Fig. 9. Distribution of heat transfer coefficient, h/h_0, for a row of 60° holes with p/D of 3.

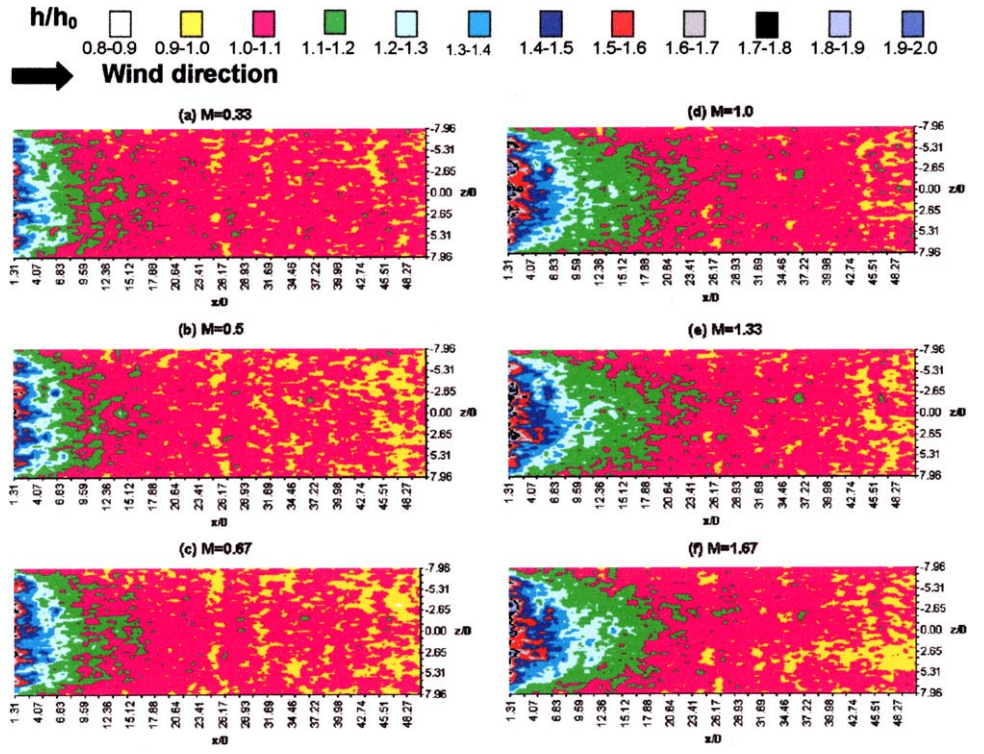

Fig. 10. Distribution of heat transfer coefficient, h/h_0, for a row of 90° holes with p/D of 3.

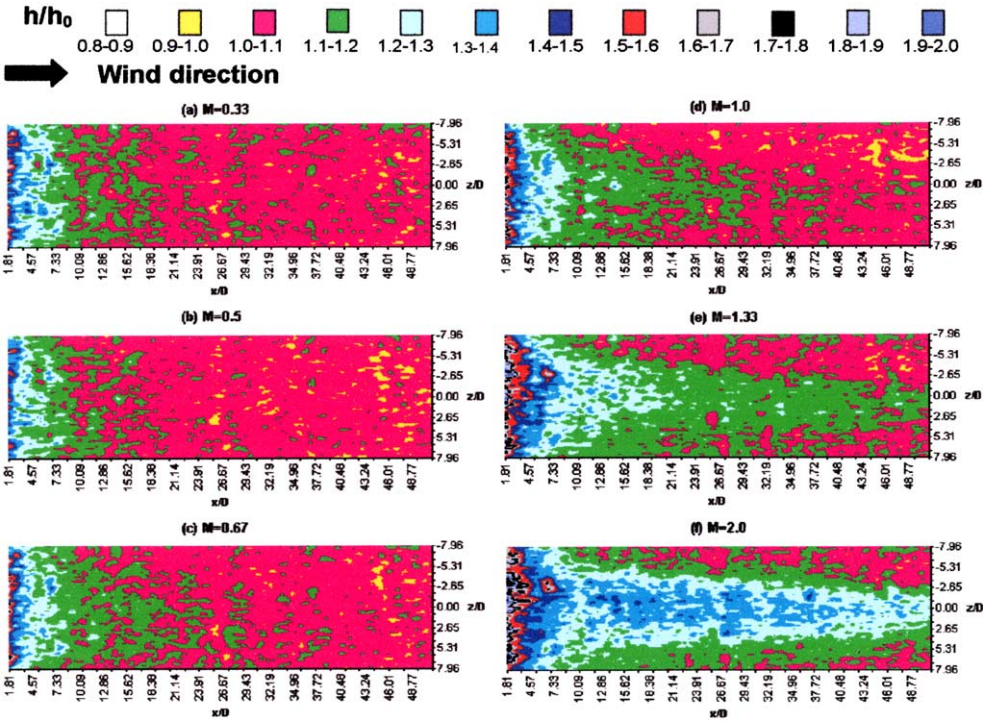

Fig. 11. Distribution of heat transfer coefficient, h/h_0, for two inline rows of 30° holes with p/D of 3 and s/D of 12.5.

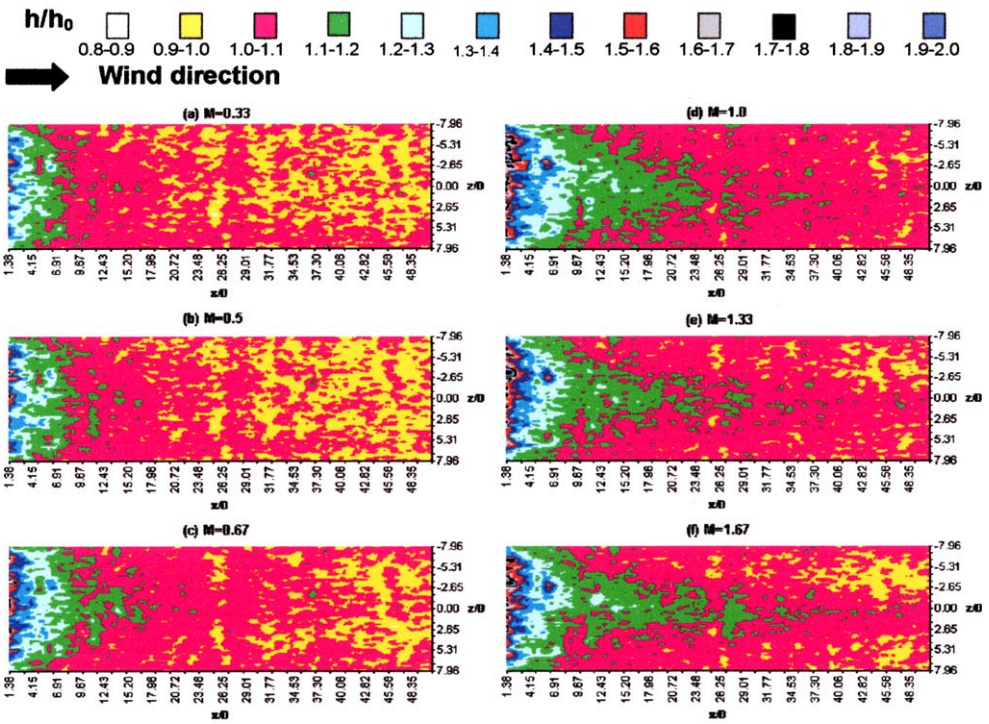

Fig. 12. Distribution of heat transfer coefficient, h/h_0, for two inline rows of 60° holes with p/D of 3 and s/D of 12.5.

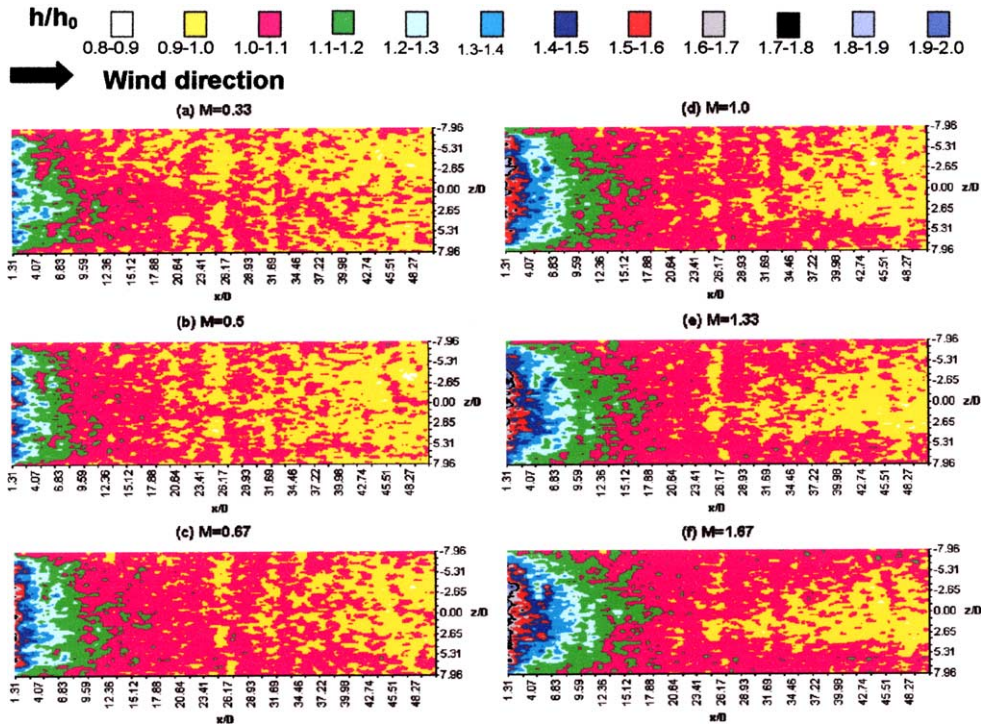

Fig. 13. Distribution of heat transfer coefficient, h/h_0, for two inline rows of 90° holes with p/D of 3 and s/D of 12.5.

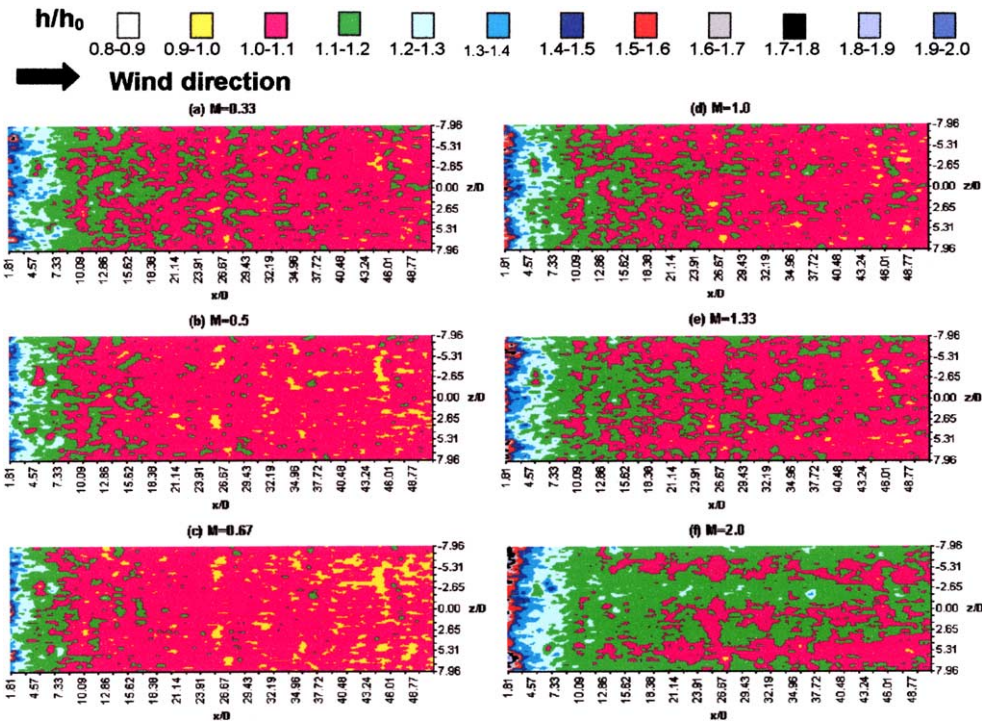

Fig. 14. Distribution of heat transfer coefficient, h/h_0, for two inline rows of 30° holes with p/D of 6 and s/D of 12.5 (only the centre 3 jets are shown).

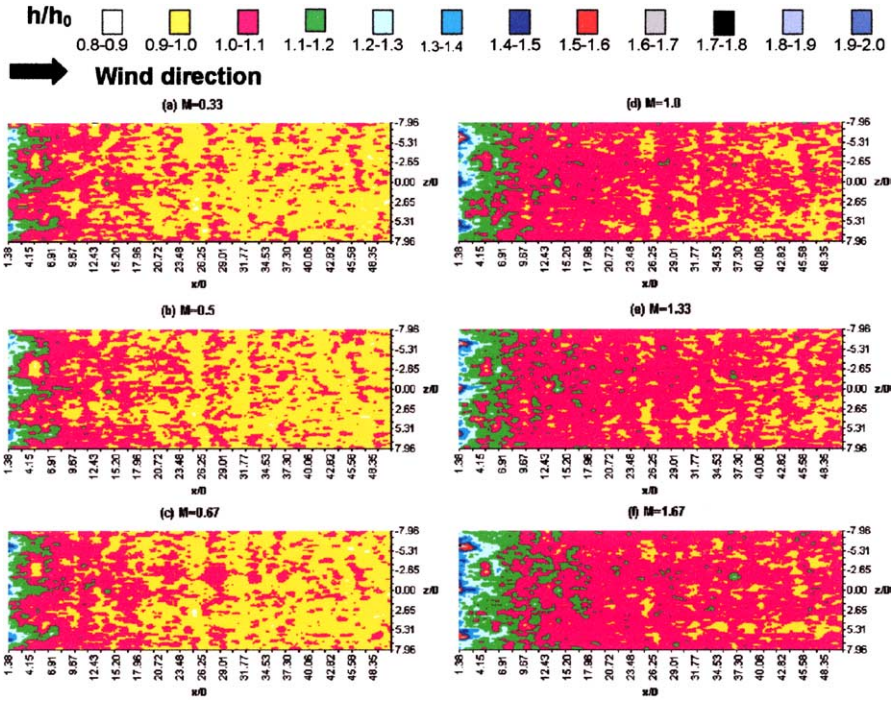

Fig. 15. Distribution of heat transfer coefficient, h/h_0, for two inline rows of 60° holes with p/D of 6 and s/D of 12.5 (only the centre 3 jets are shown).

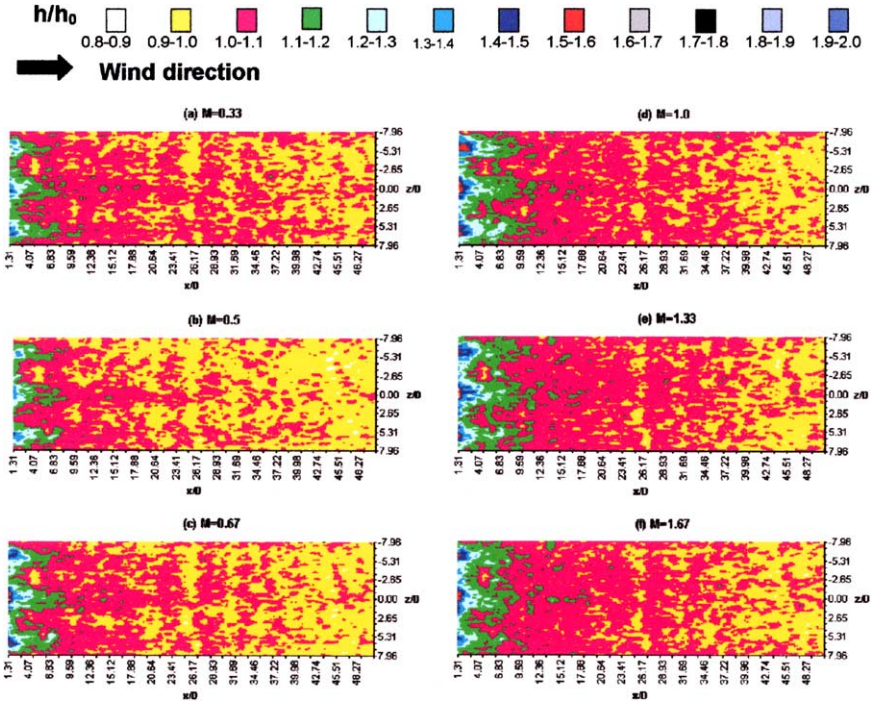

Fig. 16. Distribution of heat transfer coefficient, h/h_0, for two inline rows of 90° holes with p/D of 6 and s/D of 12.5 (only the centre 3 jets are shown).

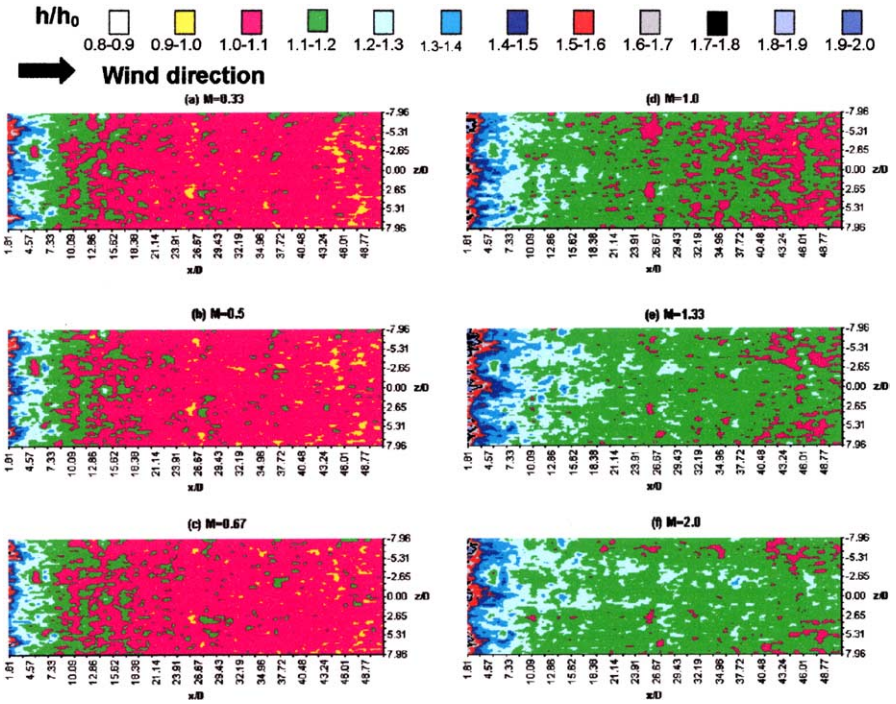

Fig. 17. Distribution of heat transfer coefficient, h/h_0 for two staggered rows of 30° holes with p/D of 6 and s/D of 12.5 (only the centre 3 jets are shown).

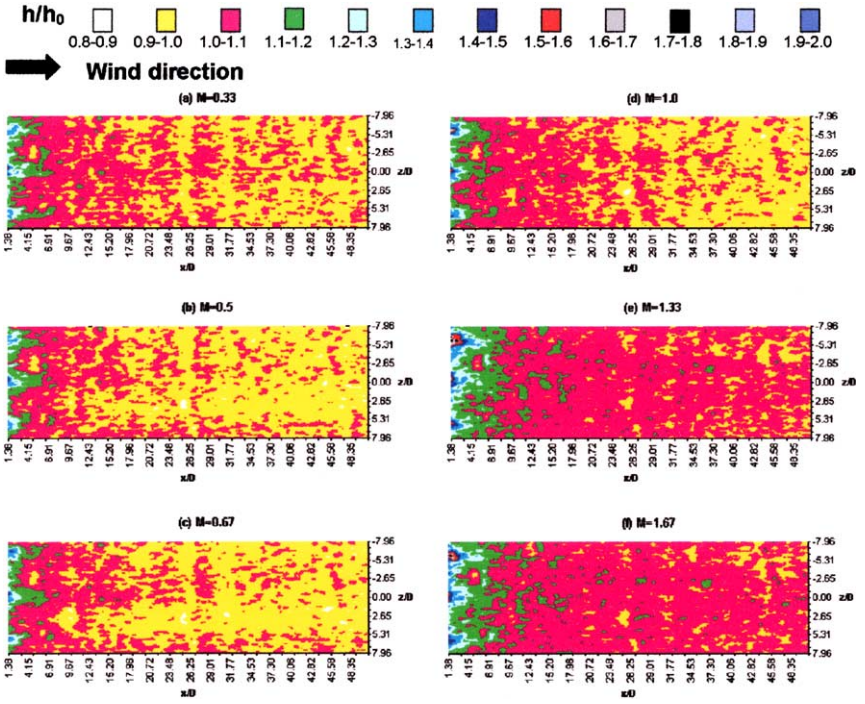

Fig. 18. Distribution of heat transfer coefficient, h/h_0, for two staggered rows of 60° holes with p/D of 6 and s/D of 12.5 (only the centre 3 jets are shown).

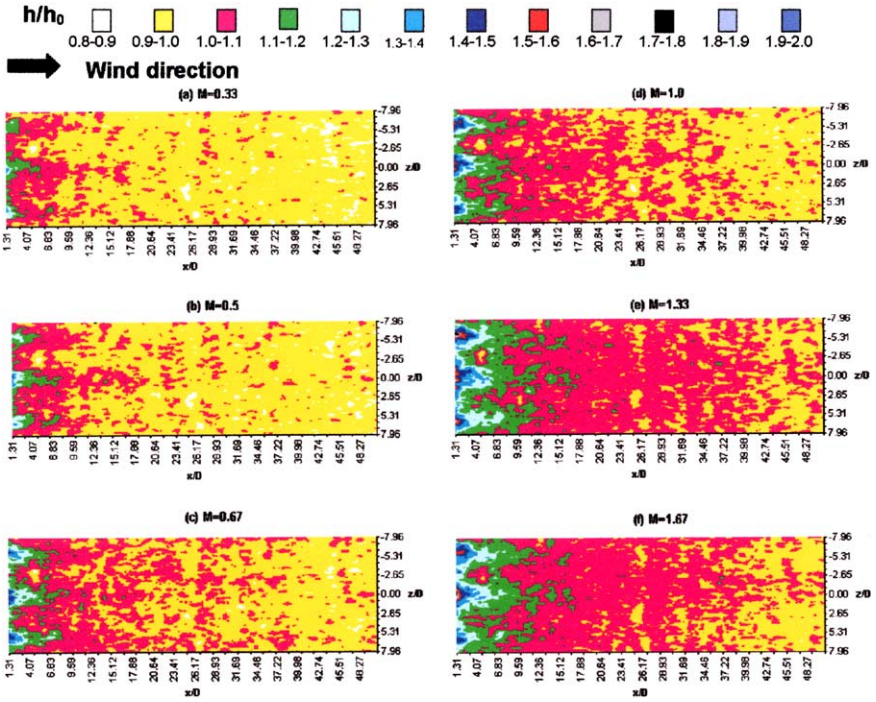

Fig. 19. Distribution of heat transfer coefficient, h/h_0, for two staggered rows of 90° holes with p/D of 6 and s/D of 12.5 (only the centre 3 jets are shown).

(K), and T_∞ is the freestream temperature (K). From this figure it is possible to infer the uncooled heat transfer coefficient, h_0, that will be used to non-dimensionalise the results in the following section.

3. Results

The axial position for the row of holes was the same as that for a single hole in Yuen and Martinez-Botas [1,2], with x/D originating from the centre of the central hole in the downstream row, and z/D from the centreline of the central hole, Fig. 1. In the results presented here, the axial range is classified into four regimes for clarity: the immediate region for $x/D \leqslant 3$, the near field for $3 \leqslant x/D \leqslant 7$, the intermediate region for $7 \leqslant x/D \leqslant 26$, and the far downstream region for $x/D \geqslant 26$.

3.1. A single row of holes

3.1.1. At 30°, 60° and 90°

The distribution of heat transfer coefficients with the row of 30° holes and a pitch-to-diameter ratio of 6 is shown in Fig. 5. The values in the immediate region downstream of the row were not significantly different to those with a single 30° hole of Yuen and Martinez-Botas [2], but the interaction between the adjacent jets increased with downstream distance and promoted heat transfer from the heated wall with a 10% increase in h/h_0 value far downstream.

Figs. 6 and 7 show contours of h/h_0 with one row of 60° and 90° holes respectively, and a pitch-to-diameter ratio of 6. The general trend of $h_{30°} > h_{60°} > h_{90°}$ found with a single hole in the previous study [2] was maintained here for similar reasons. The centreline value with the 90° holes, Fig. 7, was approximately 1.3 in the immediate region with a blowing ratio of 0.33, which was 0.4 less than that with the 60° holes. The value with the 90° holes in the immediate region was some 0.1 less than that with the 60° holes with blowing ratios greater than 0.5, and the coverage was narrower than that with the 60° which, was in turn, narrower than that with the 30° holes.

3.1.2. Effects of hole spacing

Fig. 8 presents the distribution of dimensionless heat transfer coefficients and shows that one row of 30° holes with a pitch-to-diameter ratio of 3, gave around 10% larger values than the single hole [2] at centreline positions. The values were higher at finite radii for the intermediate and large blowing ratios, consistent with the findings of Ammari et al. [7], and around 8% larger than one row with a pitch-to-diameter ratio of 6 at x/D greater than 11 and a blowing ratio of 2, Fig. 5, due to the greater jet interaction with the smaller pitch.

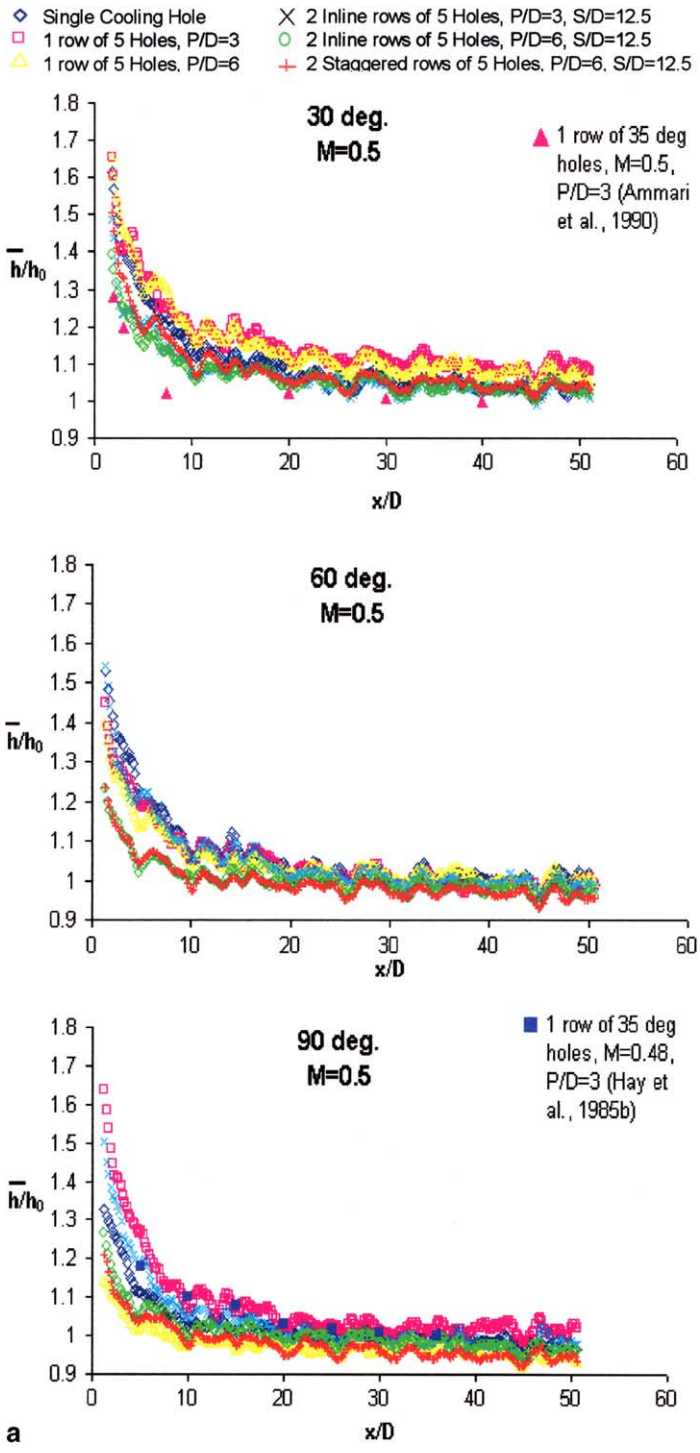

Fig. 20. (a) Variations of laterally averaged heat transfer coefficient, $\bar{h}/h_0$, with blowing ratio for 30°, 60° and 90° single holes, single rows and double rows. (b) Variations of laterally averaged heat transfer coefficient, h/h_0, with blowing ratio for 30°, 60° and 90° single holes, single rows and double rows. (c) Variations of laterally averaged heat transfer coefficient, h/h_0, with blowing ratio for 30°, 60° and 90° single holes, single rows and double rows.

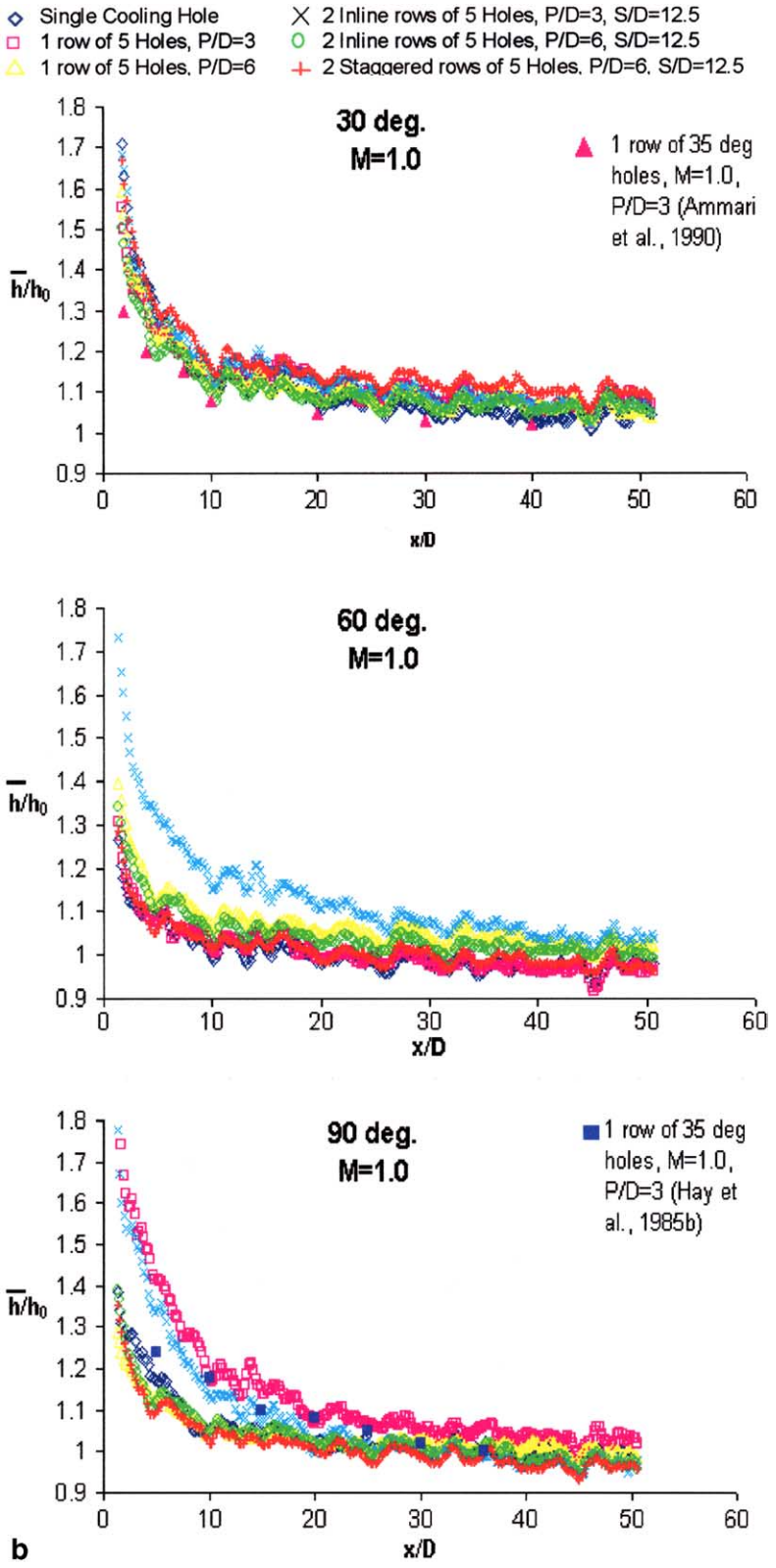

Fig. 20 (*continued*)

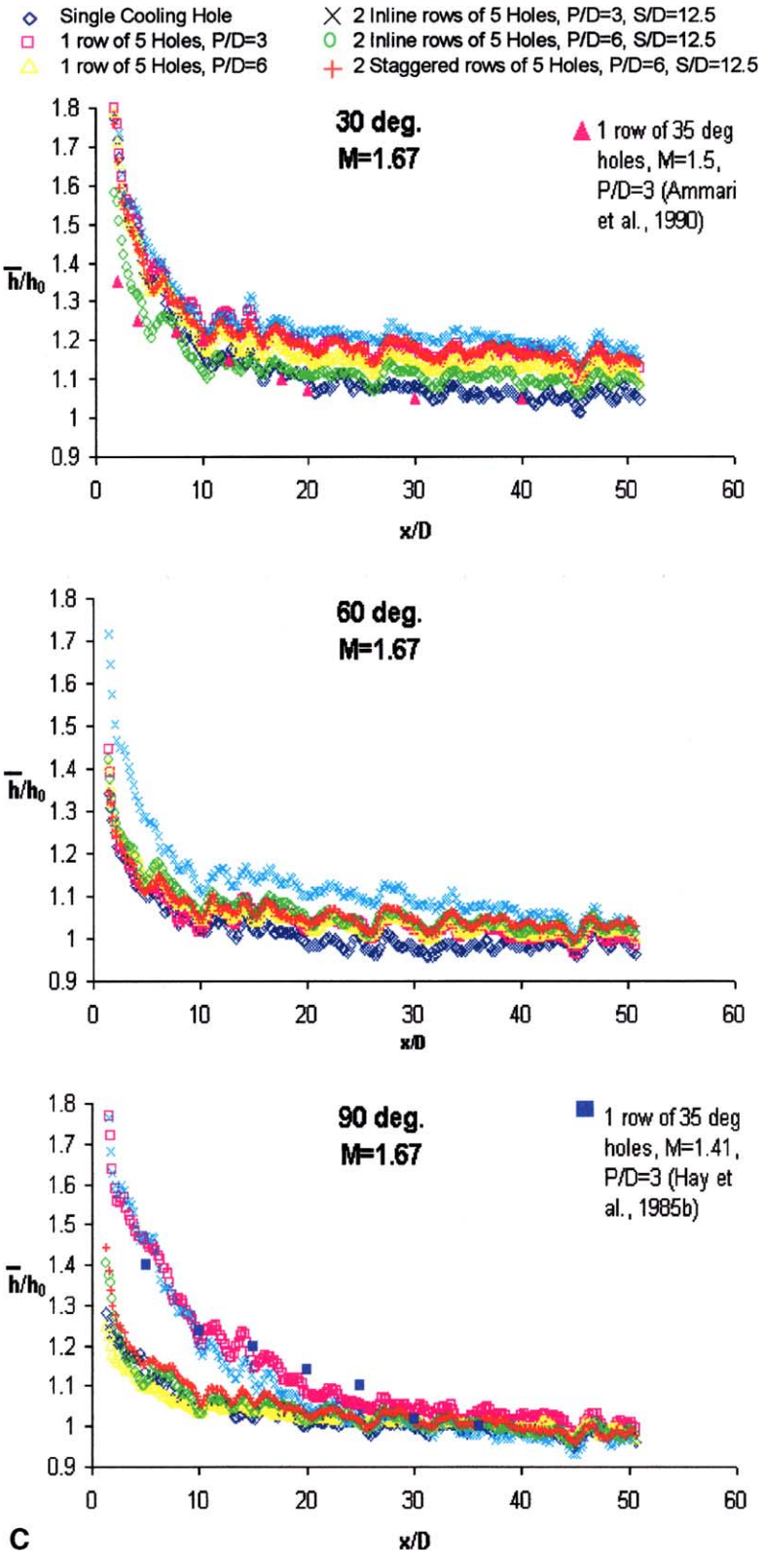

Fig. 20 (*continued*)

Fig. 9 presents the distribution of h/h_0 with one row of 60° holes and a pitch-to-diameter ratio of 3, and shows that the results are similar to those with a pitch-to-diameter ratio of 6, Fig. 6, in the immediate region, but with slightly less coverage of h/h_0 than in Fig. 6. The maximum value was 1.65, which was similar to that of Baldauf et al. [22] whose density ratio was 1.8.

Fig. 10 shows the distribution of h/h_0 with one row of 90° holes and a pitch-to-diameter ratio of 3. The h/h_0 values with the 90° holes were higher than the 60° holes, but were similar to those with the 30° holes, Fig. 8, at x/D less than 11. Comparison between Fig. 8 with one row of 30° holes and a pitch-to-diameter ratio of 3, and Fig. 10 reveals a stronger dependence on the jet-to-mainstream momentum-flux ratio with the 30° holes, in particular for blowing ratios equal to, or greater than unity, which was similar to the findings of Ammari et al. [7].

3.2. Two rows of holes

Fig. 11 shows the distribution of h/h_0 with two inline rows of 30° holes, a pitch-to-diameter ratio of 3 and a row spacing-to-diameter ratio of 12.5. The large h/h_0 values at a blowing ratio of 2 and x/D greater than 11 may reflect the large increase in effectiveness observed in [3] and relate to jet reattachment. The two inline rows of 30° holes with a pitch-to-diameter ratio of 3 gave smaller h/h_0 values than the corresponding single row in Fig. 8 for blowing ratios less than unity, and for a given injected mass flow. These findings were also noted in the comparison between the two inline rows of 30° holes and the corresponding row with a pitch-to-diameter ratio of 6 in Figs. 14 and 5 respectively.

Figs. 12 and 13 show the distributions of h/h_0 with two inline rows, a pitch-to-diameter ratio of 3 and a row spacing-to-diameter ratio of 12.5 for the 60° and 90° holes respectively, and reveal that the steeper jets gave shorter h/h_0 coverage than the 30° jets. Comparison between the two inline rows of 60° holes with a pitch-to-diameter ratio of 3 and the corresponding single row of the same angle and pitch, Fig. 9, shows that the upstream row increased the h/h_0 value at a given streamwise location and blowing ratios equal to, or greater than 0.67. However, the two inline rows gave similar values to the corresponding single row for the same injected mass flow. Comparison between the inline rows of 90° holes with a pitch-to-diameter ratio of 3 and the corresponding single row of the same angle and pitch, Fig. 10, shows little change in h/h_0 and coverage, but the comparison based on injected mass flow reveals that the two inline rows of 90° holes produced lower h/h_0 values.

Fig. 14 presents the distribution of h/h_0 with two inline rows of 30° holes and a pitch-to-diameter ratio of 6. Values of h/h_0 greater than 1.2 were achieved for x/D less than 15, and the variation was small compared to the corresponding effectiveness distribution shown in the companion paper [3]. Figs. 15 and 16 present the distributions of h/h_0 with two inline rows of 60° and 90° holes with a pitch-to-diameter ratio of 6 respectively. Values of h/h_0 greater than 1.2 remained within 10 diameters and the results were similar for both cases. The 60° and 90° holes decreased the values by around 10% compared to the 30° holes.

Fig. 17 shows the distribution of h/h_0 with two staggered rows of 30° holes and a pitch-to-diameter ratio of 6, for blowing ratios ranging from 0.33 to 2. The variation of h/h_0 with streamwise distance resembles that with the two inline rows and the same pitch-to-diameter ratio for low blowing ratios in Fig. 14, but the staggered rows gave larger values than the inline jets when the blowing ratio exceeded unity, despite of the improved spanwise uniformity in effectiveness shown in the companion paper [3]. Figs. 18 and 19 present the distributions of h/h_0 with two staggered rows of 60° and 90° holes respectively. The distributions of h/h_0 are similar, and their values are less than those with the 30° holes by approximately 15% in the immediate and near field regions.

4. Summary and concluding remarks

The distributions of $\bar{h}/h_0$ are summarised for blowing ratios of 0.5, 1 and 1.67 in Fig. 20(a)–(c). The $\bar{h}/h_0$ values decreased for the first 10 diameters downstream of the hole, and tended to unity far downstream. In general, the blowing ratio was found to have little influence on h/h_0 except for x/D less than 11. The results of Hay et al. [6] and Ammari et al. [7] with a row of 35° and 90° holes, a pitch-to-diameter ratio of 3, a density ratio of unity and the mass transfer method, are included in Fig. 20(a)–(c), and show similar trends to those reported here. Their values were lower, however, probably due to the large difference in the length-to-diameter ratio, as explained previously and in Yuen and Martinez-Botas [2].

The 30° holes gave the largest h/h_0 values with a row of holes and a pitch-to-diameter ratio of 6 for blowing ratios from 0.33 to 1.67 at all axial locations, followed by the 60° and 90° holes, in descending order. The results of Baldauf et al. [22] support the findings that the steeper jets gave lower values at moderate and high blowing ratios, and attributed this to the reduced surface interaction of the jets due to the higher jet trajectory.

The row of 90° holes with a pitch-to-diameter ratio of 3 gave larger h/h_0 values compared to the 60° holes of the same pitch, which was probably caused by the greater shear due to the higher velocity gradient, which increased the heat transfer from the wall. The combination of the relatively large heat transfer coefficient and low effectiveness provided by the 90° jets seen in [3]

suggests that they should only be used in situations where shallower injections are not feasible, for example, near the leading edge of a turbine blade where, with low blowing rates, the oncoming flow tends to ensure they remain close to the surface.

The h/h_0 values with the inline rows of holes were generally less than those given by the corresponding single row of the same pitch for a given blowing ratio, and injected mass flow. The effectiveness and coverage with the two inline rows were observed to be generally better than one row even for the same injected mass flow in the companion paper [3]. The combined performance of effectiveness and heat transfer coefficient suggests that the two inline rows are likely to be advantageous in the film cooling of turbine blades with good coverage per unit mass flow of cooling air and lower thermal stresses due to the smaller heat load.

The staggered rows improved the spanwise uniformity in effectiveness, but the h/h_0 values were larger than those with the inline rows of the same pitch for all blowing ratios with the 30° holes.

Acknowledgement

The authors would like to thank Alstom Power Ltd., particularly Prof. J. Hannis, Dr. J. Turner, Dr. Gan for supporting the present work.

References

[1] C.H.N. Yuen, R.F. Martinez-Botas, Film cooling characteristics of a single round hole at various angles in a crossflow: Part I. Effectiveness, Int. J. Heat Mass Transfer, in press.

[2] C.H.N. Yuen, R.F. Martinez-Botas, Film cooling characteristics of a single round hole at various angles in a crossflow: Part II. Heat transfer coefficients, Int. J. Heat Mass Transfer, in press.

[3] C.H.N. Yuen, R.F. Martinez-Botas, Film cooling characteristics of rows of round holes at various angles in a crossflow: Part I. Effectiveness, Int. J. Heat Mass Transfer, submitted for publication.

[4] V.L. Eriksen, R.J. Goldstein, Heat transfer and film cooling following injection through inclined circular tubes, ASME J. Heat Transfer (May) (1974) 239–245.

[5] R.J. Goldstein, T. Yoshida, Boundary layer and laminar injection on film cooling performance, ASME J. Heat Transfer 104 (1982) 355–362.

[6] N. Hay, D. Lampard, C.L. Saluja, Effects of cooling films on the heat transfer coefficient on a flat plate with zero mainstream pressure gradient, J. Eng. Gas Turbines Power 107 (1985) 105–110.

[7] H.D. Ammari, N. Hay, D. Lampard, The effect of density ratio on the heat transfer coefficient from a film-cooled flat plate, ASME J. Turbomach. 112 (1990) 444–450.

[8] P.J. Loftus, T.V. Jones, The effect of temperature ratios on the film cooling process, ASME J. Eng. Power 105 (1983) 615–621.

[9] P.M. Ligrani, A. Ortiz, S.L. Joseph, D.L. Evans, Effects of embedded vortices on film-cooled turbulent boundary layers, ASME J. Turbomach. 111 (1989) 71–77.

[10] B. Sen, D.L. Schmidt, D.G. Bogard, Film cooling with compound angle holes: heat transfer, ASME J. Turbomach. 118 (1996) 800–806.

[11] J.R. Pietrzyk, D.G. Bogard, M.E. Crawford, Hydrodynamics measurements of jets in crossflow for gas turbine film cooling applications, AMSE J. Turbomach. 111 (2) (1989) 139–145.

[12] A.K. Sinha, D.G. Bogard, M.E. Crawford, Gas turbine film cooling: flowfield due to a second row of holes, ASME J. Turbomach. 113 (1991) 450–456.

[13] S.W. Burd, T.W. Simon, Measurements of discharge coefficients in film cooling, ASME Paper no. 98-GT–009, 1998.

[14] S.W. Burd, T.W. Simon, Turbulence spectra and length scales measured in film coolant flows emerging from discrete holes, ASME Paper no. 98-GT-190, 1998.

[15] A.L. Brundage, M.W. Plesniak, S. Ramadhyani, Influence of coolant feed direction and hole length on film cooling jet velocity profiles, ASME Paper no. 99-GT-35, 1999.

[16] D.K. Walters, J.H. Leylek, A detailed analysis of film cooling physics: Part I—Strearnwise injection with cylindrical holes, ASME J. Turbomach. 122 (2000) 102–112.

[17] C.H.N. Yuen, Measurement of Local Heat Transfer Coefficient and Film Cooling Effectiveness Ion Film Cooling Geometries, Ph.D. thesis, University of London, Imperial College of Science, Technology and Medicine, London, 2000.

[18] S. Lloyd, A. Brown, Fluid flow and heat transfer characteristics in the entrance region of circular pipes, ASME Paper no. 85-GT-120, 1985.

[19] G.E. Andrews, M. Alikhanizadeh, A.A. Asere, C.I. Hussain, M.S. Khoshkbar, M.S. Azari, M.C. Mkpadi, Small diameter film cooling holes: wall convective heat transfer, ASME J. Turbomach. 108 (1986) 283–289.

[20] P.J. Schneider, Conduction Heat Transfer, sixth ed., Addison-Wesley, Reading, MA, 1974, pp. 176–181.

[21] S.J. Kline, F.A. McClintock, Describing uncertainties in single-sample experiments, Mech. Eng. (January) (1953) 3–8.

[22] S. Baldauf, A. Schulz, S. Wittig, High resolution measurements of local heat transfer coefficients by discrete hole film cooling, ASME Paper presented at the International Gas Turbine and Aeroengine Congress and Exhibition, Indianapolis, IN—June 7–10 1999, ASME paper 99-GT-43.